



CHORUS

This is the accepted manuscript made available via CHORUS. The article has been published as:

Deuteron breakup induced by 14-MeV neutrons from inertial confinement fusion

C. J. Forrest, A. Deltuva, W. U. Schröder, A. V. Voinov, J. P. Knauer, E. M. Campbell, G. W. Collins, V. Yu. Glebov, O. M. Mannion, Z. L. Mohamed, P. B. Radha, S. P. Regan, T. C. Sangster, and C. Stoeckl

Phys. Rev. C **100**, 034001 — Published 10 September 2019

DOI: [10.1103/PhysRevC.100.034001](https://doi.org/10.1103/PhysRevC.100.034001)

Deuteron breakup induced by 14-MeV neutrons from inertial confinement fusion

C. J. Forrest,¹ A. Deltuva,² W. U. Schroeder,^{1,3} A.V. Voinov,⁴ J. P. Knauer,¹
E. M. Campbell,¹ G. W. Collins,¹ V. Yu. Glebov,¹ O. M. Mannion,¹ Z. L. Mohamed,¹
P. B. Radha,¹ S. P. Regan,¹ T. C. Sangster,¹ and C. Stoeckl¹

¹*Laboratory for Laser Energetics, University of Rochester, 250 East River Road*

Rochester, New York 14623-1299, USA

²*Institute of Theoretical Physics and Astronomy, Vilnius University, Vilnius LT-10257,*

³*Departments of Chemistry and Physics, University of Rochester, Rochester, New York
14627, USA*

⁴*Ohio University, Athens, OH 45701, USA*

Measurements are reported for the angle-averaged double-differential cross section $\langle d^2\sigma/dE_n d\Omega_n \rangle_{0^\circ < \theta < 7.4^\circ}$ for the breakup reaction ${}^2\text{H}(n,2n){}^1\text{H}$, induced by 14-MeV neutrons generated using an inertial confinement fusion platform. A bright neutron source, created on the OMEGA Laser System [T. R. Boehly *et al.*, Opt. Commun. **133**, 495 (1997)] with a luminosity of $L = 10^{24} \text{ s}^{-1}$, was used to irradiate deuterated targets. The absolute yields and energy spectra from the breakup neutrons emitted in a forward-angle geometry ($\theta = 0^\circ$ to 7.4°) were detected with a sensitive, high-dynamic-range neutron time-of-flight spectrometer. The cross-section data, measured for neutron energy range from 0.5- to 10-MeV, are well reproduced by theoretical model calculation employing realistic nucleon–nucleon and three-nucleon forces.

I. INTRODUCTION

Few-nucleon systems and reactions between light nuclei continue to attract interest since they provide testing grounds for modern microscopic nuclear theory. Numerous experiments conducted over the past several decades have searched for evidence of a three-nucleon force (3NF) in addition to the nucleon–nucleon (NN) interactions [1]. The under binding energies for ${}^3\text{H}$ and ${}^3\text{He}$ is one example of convincing evidence for a 3NF [2]. It has been shown that the binding energies of these nuclei cannot be reproduced by solutions of the corresponding Faddeev equations employing only traditional NN forces [3]. Furthermore, three-nucleon effects have been reported in the theoretical analysis of deuteron breakup [4].

Studying the deuteron breakup has several advantages. In particular, neutron-induced scattering and reactions with deuterons, where the Coulomb force is absent, are useful for theoretical analysis with realistic NN or 3NF, in both the elastic and breakup channels. In the past, discrepancies between theory and data were attributed to the inadequate NN and 3N force models that were used to explain the measurements [5]. In this work, the experimental data can be only explained by modern calculations including 3N forces.

Exact numerical solutions of neutron–deuteron Faddeev equations have been obtained by several research groups [4,6]. In the present work, an extended force model using realistic (CD Bonn + Δ + U1) [7] potentials in addition to NN and 3N forces considers also the excitation of a nucleon into a Δ isobar, thereby yielding an effective 3NF, consistent with the underlying two-baryon potential. The availability of these exact 3N calculations using realistic potentials allows one to examine 3NF effects. Previous

experiments have reported on cross-section measurements of the breakup of a deuteron in the region far from the final-state-interaction (FSI) peak, which is sensitive only to the scattering length a_{NN} . In these past measurements a significant difference as compared to the available calculations in the evaluated nuclear libraries (Nuclear Data Services) was observed [8–10]. Therefore, it is necessary to measure the reaction in the region far from the FSI dominance, where the cross section may be more sensitive to the 3NF effect.

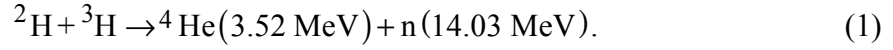
There is an additional, more-specialized aspect of studying the neutron-induced process with deuterons. Active research in thermonuclear fusion energy also requires accurate cross sections for neutron-induced breakup reaction of deuteron and triton to better understand the neutron energy spectrum produced in inertial confinement fusion (ICF) experiments that consist of cryogenic deuterium–tritium fuel [11]. Precise knowledge of the neutron contributions from thermonuclear and scattering reactions that comprise the energy spectrum is crucial to understanding the dynamics of the fuel assembly at peak compression [12]. This includes the double-differential cross section caused by the inelastic scattering of n - ^2H at 14 MeV off the cold fuel in this class of implosions, which is a significant component in the measured energy spectrum. For this reason, the neutron contribution from the inelastic scattering of deuterium in this energy region must be known to within $\approx 5\%$ to accurately model the neutron energy spectrum to determine implosion performance metrics. It should also be mentioned that the breakup reaction of a triton is equally important to understanding the complete energy spectrum and is currently being investigated using a similar technique as described here and will be reported in a future publication.

This paper reports on the first measurement of the deuteron breakup using a new laser-based ICF platform developed on the Omega Laser System. The cross section was inferred with an emission angle of the breakup neutrons from the reaction vessel accepted by the diagnostic of $0^\circ \leq \theta \leq 7.4^\circ$, $0^\circ \leq \varphi \leq 2\pi$ with an energy range between 0.5 MeV and 10.0 MeV, which is over a larger region than achieved in earlier accelerator experiments. The measured cross section from the experimental campaigns on OMEGA is well reproduced by rigorous calculations of the double-differential cross section in the energy region below the FSI peak. Details of the experimental setup and analysis methods are reported in this paper.

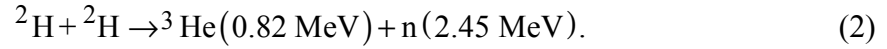
II. EXPERIMENTAL DETAILS

A high-intensity pulse of 14-MeV neutrons produced from direct-drive ICF implosions on the OMEGA Laser System with a luminosity of $L = 10^{24} \text{ s}^{-1}$ at the University of Rochester's Laboratory for Laser Energetics [13] is used to irradiate axially symmetric vessels that contain either a deuterated or a corresponding non-deuterated target. Both elastic scattering and inelastic reactions are measured through the detection of neutrons using a highly collimated spectrometer in line with the reaction vessel. Evidence of the deuteron breakup is inferred from the difference in the signal between the deuterated and non-deuterated targets. A general schematic of the OMEGA target chamber, a highly collimated line-of sight, and the neutron time-of-flight (nTOF) experimental setup is shown in Fig. 1.

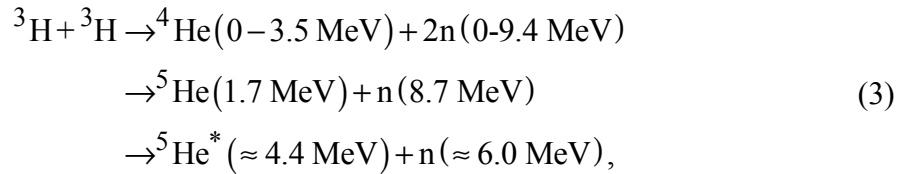
In direct-drive ICF experiments, neutrons are generated using a laser to implode microballoons filled with D-T fuel¹. The dominant fusion reaction in these implosions is [14].



Two additional primary fusion reactions [14],



and



have a much smaller contribution due the yield produced ($\approx 10^{-2}$) and lower neutron energies compared to the primary fusion reaction yield, which results in a minimal impact on the experimental data presented in this paper.

The bright ICF neutron source (14 MeV) generated for this experiment uses a specific type of ICF target with a thin-walled ($\approx 4\text{-}\mu\text{m}$), $\approx 1\text{-mm}$ -diam SiO_2 microballoon filled with 10 atm of equimolar D-T fuel [15]. The OMEGA UV laser's 60 beams deliver

¹ D-T (deuterium-tritium) denote ${}^2\text{H}$ and ${}^3\text{H}$, respectively.

up to 30 kJ of energy onto the ICF target during a nominal 1-ns square pulse. The symmetric illumination rapidly heats the thin shell of the microballoon, causing it to expand, resulting in a shock wave that is driven into the fuel [16]. This shock wave compresses and heats the fuel as it converges at the center of the target. As the shock rebounds, the fuel reaches sufficient temperatures (i.e., ≈ 10 keV) to produce thermonuclear reactions with neutron yields of up to 1×10^{14} emitted into 4π . In this ICF implosion design, the “bang time” (time when peak neutron production takes place) is ≈ 800 ps after the laser pulse hits the target with a neutron-production rate of ≈ 100 ps [17]. The neutron-emitting region (hot spot) for this class of implosions is ≈ 100 μm in diameter.

The nuclear reaction vessel (NRV) is constructed from thin-wall (1-mm) aluminum to minimize residual neutron scattering. The overall length of the truncated cone-shaped vessel is 7.5 cm, with a smallest diameter of 0.9 cm and a largest diameter of 4 cm. The vessel was specially designed to be positioned 9 cm from the center of the OMEGA target chamber to ensure that the laser beams have a clear path to illuminate the microballoon. The vessel can be attached to a specially designed bracket mounted in one of the ten-inch manipulator diagnostic ports on the target chamber. The neutrons emitted from the breakup of the deuteron are measured in the angular region of $0^\circ \leq \theta \leq 7.4^\circ, 0^\circ \leq \varphi \leq 2\pi$ as a result of the geometry of the reaction volume with respect to the diagnostic instrument. The emitted neutrons are recorded in current mode using a time-of-flight spectrometer with a large dynamic range, located along the clear line-of-sight axis downstream of the reaction vessel. The diagnostic used to measure the neutron energy spectrum in this campaign is a four-microchannel-plate photomultiplier

tube (MCP-PMT) detector positioned 13.4 m from target chamber center. It consists of a 20-cm-diam, 10-cm-deep stainless-steel cylindrical cell that contains the scintillation fluid viewed perpendicular by the four PMT's outside the line of sight. This detector uses a thin-wall (2-mm) construction to minimize neutron scattering by the scintillator housing. Thin (<0.3-cm) stainless-steel end plates are used to seal the cylindrical cell to minimize neutron attenuation. The ports for the MCP-PMT are 40-mm-diam fused-silica windows mounted on the cylindrical cell and sealed with Viton O rings. The cell is filled with a liquid scintillator based on oxygenated xylene doped with diphenyloxazole $C_{15}H_{11}NO$ + p-bis-(o-methylstyryl)-benzene (PPO+ bis-MSB) wavelength-shifting dyes, which scintillates and emits light in the visible to near-ultraviolet wavelength range (i.e., from 380 nm to 420 nm). This oxygenated liquid scintillator has a fast time response and a low-light afterglow, which is required to measure lower-energy (<1-MeV) neutrons [18]. The detector is shielded from scattered background neutrons using a mid-beam collimator constructed from high-density polyethylene and the 1-m-thick concrete floor. A schematic of the experimental setup of the reaction vessel with respect to the diagnostic is shown in Fig. 2. The primary D-T neutron yield signal from a separate (monitor) standard diagnostic, which has an uncertainty of 5%, is used to absolutely calibrate the spectrometer [19].

III. DATA ANALYSIS

The first set of experiments used vessels that contained deuterated compounds such as D_2O and C_6D_6 to investigate the breakup of deuterons. A separate set of vessels in these experiments were filled with standard non-deuterated target compounds (H_2O ,

C_6H_6) to identify contributions from the inelastic neutron scattering on oxygen and carbon in the NRV. For each reaction vessel, up to six implosions generating a neutron luminosity of $L = 10^{24} \text{ s}^{-1}$ were performed for both the non-deuterated and the deuterated samples. The primary D-T neutron signal from the monitor diagnostic was used to normalize the measured breakup neutron signal with respect to the primary yield for each implosion. Signals that used a specific vessel were averaged to enhance the signal-to-noise ratio. A comparison of the spectra obtained with the vessels filled with the deuterated and non-deuterated compounds clearly shows the contribution from the neutron-induced breakup in the time-of-flight region: 300 ns (≈ 14 MeV) to 600 ns (≈ 2.5 MeV), as seen in Fig. 3. In both cases, the measured yield of neutrons generated in the breakup reaction are affected identically by additional absorption and scattering effects in the target material. For example, the two excited oxygen states (6.1, 7.0 MeV) are seen in spectra measured with the H_2O and D_2O vessels, and several excited states of carbon (4.44, 7.65, 9.64 MeV) are observed in the spectra from the C_6H_6 and C_6D_6 vessels.

The neutron yield from the deuteron-breakup contribution is extracted using the difference in the time-of-flight spectra obtained from the deuterated and the corresponding non-deuterated vessel. This method is advantageous since it removes the background contributions from inelastic scattering off both carbon and oxygen, along with any additional scattering and nonlinearity in the detection system that arise from the experimental configuration; it also demonstrates the sensitivity in the signals. The residual signal from the subtraction has been shown to originate from the neutron-induced breakup reaction [20]. With the neutron yield attributed to the neutron-induced

breakup reaction, the double-differential cross section is calculated using the following relation:

$$\frac{d^2 Y_{n,2n}}{dE d\Omega_{\text{dia}}(x_{\text{NRV}})} = m_n n_d \int_0^{l_{\text{NRV}}} Y_{\text{inc}}(x_{\text{NRV}}) \frac{d^2 \sigma_{n,2n}}{d\Omega dE} Y_{\text{NRV}}(E, x_{\text{NRV}}) \varepsilon_{\text{dia}}(E) dx_{\text{NRV}},$$

where

- $Y_{n,2n}$ = the number of detected neutrons from the neutron-induced breakup reaction
- m_n = the multiplicity for the number of generated neutrons from the breakup ($m_n = 2$)
- n_D = the number density of deuterium in the reaction vessel
- l_{NRV} = length of the reaction vessel
- $\Omega_{\text{dia}}(x_{\text{NRV}})$ = solid angle of the detector at x_{NRV}
- $Y_{\text{inc}}(x_{\text{NRV}})$ = the number of incident 14.03-MeV neutrons at x_{NRV}
- $d^2 \sigma_{n,2n} / d\Omega dE$ = double-differential cross section for the neutron-induced breakup reaction
- $\tau_{\text{NRV}}(E, x_{\text{NRV}})$ = transmission of neutron with energy E through the reaction vessel at x_{NRV}
- $\varepsilon_{\text{dia}}(E)$ = fraction of neutrons at energy E interacting inside detector

A total experimental uncertainty of the $Y_{n,2n}$ yield measurement is derived from statistical and systematic uncertainties. The number of neutrons measured in the 13.4-m spectrometer for each 0.5-MeV energy bin is in the range between 10^4 and 10^5 , which

leads to a statistical uncertainty of $\approx 3\%$. Systematic uncertainties are associated with a number of steps involved in the calibration of the detector. A small uncertainty of the order of $\approx 1\%$ is caused by the nonlinear light output as a function incident neutron energy from the scintillation fluid. The Y_{DD} yield reference used to calibrate the nTOF spectrometer efficiency is estimated to have a systematic uncertainty of $\approx 9\%$.

A. Monte Carlo Simulations

The 14-MeV neutrons entering the scattering sample can cause the breakup reaction and can also slow down as result of multiple elastic scattering on constituent nuclei. Slowed-down neutrons with energies less than 14 MeV that induce the breakup reaction could also systematically enhance the experimentally measured cross-section values. This effect was modeled using the neutron transport code MCNP simulating details of the experimental setup [21]. The simulations included a high-yield source of 14-MeV neutrons, which were incident on the nuclear reaction vessel. In the model, an infinitely thin plane represented the surface of the nTOF spectrometer positioned at 13.4 m from the high-yield neutron source. It was determined from these simulations that multiple scattering of the neutrons in the vessel affected the measured neutron spectrum used to calculate the double-differential cross section. This is the result of incident 14-MeV neutrons that undergo a scatter event within the vessel before the breakup reaction. Simulations showed that a correction is required to infer cross section from the measurement of neutrons that were emitted in the neutron breakup by only 14-MeV neutrons in the vessel. The corrections for the different vessels can be as high as 20% in the energy region below 2 MeV, as shown in Fig. 4, where the cross section from

neutrons <14 MeV to the cross section from neutrons at 14 MeV is plotted. It should be noted that the cross section available in MCNP is derived from the n-body phase space distribution model (Law 6) used in Evaluated Nuclear Data Files (ENDF). This distribution is significantly different in shape and magnitude to the theoretical model that is compared to the experimental data reported in this paper.

IV. RESULTS AND DISCUSSION

Experimental results displayed in Fig. 5 are in much better agreement with a model calculation employing realistic NN and 3N forces over a larger energy region than achieved in past accelerator-based experiments [7]. The good agreement over a broad energy range indicates that essential aspects of the interaction dynamics are treated correctly in the model provided. This experimental technique has not matured enough, however, to measure the cross section in the region of the FSI peak at ≈ 11.8 MeV because of limitations in the current diagnostics, although the region below the final-state configuration is of particular interest since it may be more sensitive to the 3NF contributions.

The experimental angle-averaged cross section $\langle d^2\sigma/dE_n d\Omega_n \rangle$ measured in the angular range of $0^\circ \leq \theta \leq 7.4^\circ$, $0^\circ \leq \varphi \leq 2\pi$ and for neutrons between 0.5 MeV and 10.0 MeV are presented in Table I. The error on the data in Table I and Fig. 5 includes both the systematic and statistical uncertainties. In the region between 3 and 10 MeV, the measured cross sections from experiments using the different reaction vessels (D_2O , C_6D_6) are in good agreement. The region from 2 to 3 MeV was excluded because of the

presence of a strong peak at 2.45 MeV caused by the D-D fusion reaction and resulted in the low signal-to-noise in the time-of-flight spectra.

The cross-section data were compared to results of rigorous calculations from Ref. [7] using the realistic CD Bonn + Δ + U1 model. The model includes both effective 3NF because of the explicit virtual Δ isobar excitation and irreducible 3NF as shown in Fig. 5. The solid line represents the calculation with the neutron emission angle at $\langle d^2\sigma/dE_n d\Omega_n \rangle_{0^\circ < \theta < 7.4^\circ}$, respectively; however, the 3NF effect turns out to be very small. Results obtained using another realistic NN potential INOY04 [22] without explicit 3NF are indistinguishable from those shown in the plot. As compared to model calculations, the measurements exhibit a systematically lower value than predicted in the 3- to 5-MeV energy range

The cross-section measurements from this new experimental platform reported here are also compared to the previous neutron-induced breakup measurement performed on accelerators [9, 10]. Earlier data sets are plotted [see Fig. 5(b)] with only the statistically uncertainty (5%) as provided by the ENDF nuclear libraries. These experiments inferred a marginally lower cross section between 4 and 10 MeV as compared to the recent *ab initio* calculation. In addition, these earlier experiments from Refs. [9,10] do not show a separation consistent with the different neutron emission angles of 0° and 7° , respectively.

Several past experiments on the breakup of deuterons have primarily focused on the FSI peak and the phase space of the three-body breakup referred to as the quasi-free scatter region to study nucleon-nucleon forces [23]. However, it has been suggested that the collinearity case could be a third prominent region in the phase space that might

exhibit characteristic behavior and could be of interest in understanding three-nucleon interactions. In the collinear situation, one of the nucleons is left at rest in the center-of-mass frame, while the remaining two nucleons are emitted with opposite linear momentum. This particular geometry, collinearity of the outgoing nucleons, could highlight shielding effects of a possible three-body force with two-meson exchange [24]. This effect received much attention in past experiments that measured the proton-induced breakup of deuterons [25]. However, the cross section enhancement was only observed in an experiment with $E_p = 156$ MeV, albeit with low statistics [26]. The experimental data reported in this paper do not show evidence for an enhancement in collinearity behavior of the cross section ≈ 1.7 MeV, which has been suggested in previous experiments [27].

V. SUMMARY AND CONCLUSIONS

In summary, a novel laser-based ICF-driven platform that provides a bright source of 14-MeV DT neutrons with a luminosity of $L = 10^{24}$ s⁻¹ was used to irradiate deuterated targets and measure the cross section from the breakup reaction. Contributions from the neutron-induced deuteron breakup were observed from the difference in spectra obtained from a deuterated and the corresponding non-deuterated reaction vessel. The angle-averaged double-differential cross section $\langle d^2\sigma/dE_n d\Omega_n \rangle_{0^\circ < \theta < 7.4^\circ}$ was measured over a larger region of energy (0.5 to 10 MeV) than achieved in previous accelerator measurements. Each data point has a statistical uncertainty of less than 3% between 3 and 10 MeV. The systematic uncertainty of the present data is 9%.

Rigorous Faddeev-type calculation of the neutron-induced deuteron breakup using the realistic CD Bonn + Δ + U1 model, which includes genuine 3NF and effective 3NF

effects because of the Δ isobar excitation, reproduces well the experimental data for neutron energies below the FSI peak; the 3NF effect is, however, insignificant. However, the experimental data exhibit systematically lower values in the 3- to 5-MeV energy range.

ACKNOWLEDGMENT

The authors thank the OMEGA operations crew for their help in executing these experiments. This material is based upon work supported by the Department of Energy National Nuclear Security Administration under Award Number DE-NA0003856, the University of Rochester, and the New York State Energy Research and Development Authority. The work of Arnoldas Deltuva was supported by the Alexander von Humboldt-Foundation under Grant No. LTU-1185721-HFST-E. The work of Alexander Voinov was supported by the Department of Energy, grant number DE-NA0002905 and Lawrence Livermore National Laboratory, subcontract number B610277.

This report was prepared as an account of work sponsored by an agency of the U.S. Government. Neither the U.S. Government nor any agency thereof, nor any of their employees, makes any warranty, express or implied, or assumes any legal liability or responsibility for the accuracy, completeness, or usefulness of any information, apparatus, product, or process disclosed, or represents that its use would not infringe privately owned rights. Reference herein to any specific commercial product, process, or service by trade name, trademark, manufacturer, or otherwise does not necessarily constitute or imply its endorsement, recommendation, or favoring by the U.S.

Government or any agency thereof. The views and opinions of authors expressed herein do not necessarily state or reflect those of the U.S. Government or any agency thereof.

References

1. E. S. Konobeevski, S. V. Zuyev, M. V. Mordovskoy, S. I. Potashev, and I. M. Sharapov, *Phys. At. Nucl.* **76**, 1398 (2013).
2. A. Nogga, H. Kamada, and W. Glöckle, *Phys. Rev. Lett.* **85**, 944 (2000).
3. C. R. Chen, G. L. Payne, J. L. Friar, and B. F. Gibson, *Phys. Rev. C* **33**, 1740 (1986); S. Ishikawa and T. Sasakawa, *Few-Body Syst.* **1**, 143 (1986).
4. J. Kuroś-Żołnierczuk, H. Witała, J. Golak, H. Kamada, A. Nogga, R. Skibiński, and W. Glöckle, *Phys. Rev. C* **66**, 024004 (2002).
5. H. R. Setze, C. R. Howell, W. Tornow, R. T. Braun, D. E. González Trotter, A. H. Hussein, R. S. Pedroni, C. D. Roper, F. Salinas, I. Šlaus *et al.*, *Phys. Rev. C* **71**, 034006 (2005).
6. A. Deltuva, K. Chmielewski, and P. U. Sauer, *Phys. Rev. C* **67**, 034001 (2003).
7. A. Deltuva and P. U. Sauer, *Phys. Rev. C* **91**, 034002 (2015).
8. P. G. Young, G. M. Hale, and M. G. Chadwick, ENDF/B-VII.1, IAEA Nuclear Data Services, 22 December 2011.
9. M. Brüllmann, H. Jung, D. Meier, and P. Marmier, *Phys. Lett. B* **25**, 269 (1967).
10. J. Kecskeméti, T. Czibók, and B. Zeitnitz, *Nucl. Phys. A* **254**, 110 (1975).
11. J. Nuckolls, L. Wood, A. Thiessen, and G. Zimmerman, *Nature* **239**, 139 (1972).
12. S. P. Regan, V. N. Goncharov, I. V. Igumenshchev, T. C. Sangster, R. Betti, A. Bose, T. R. Boehly, M. J. Bonino, E. M. Campbell, D. Cao, *et al.*, *Phys. Rev. Lett.* **117**, 025001 (2016); **117**, 059903(E) (2016).

13. T. R. Boehly, D. L. Brown, R. S. Craxton, R. L. Keck, J. P. Knauer, J. H. Kelly, T. J. Kessler, S. A. Kumpan, S. J. Loucks, S. A. Letzring *et al.*, *Opt. Commun.* **133**, 495 (1997).
14. S. Atzeni and J. Meyer-ter-Vehn, *The Physics of Inertial Fusion: Beam Plasma Interaction, Hydrodynamics, Hot Dense Matter*, 1st ed., International Series of Monographs on Physics, Vol. 125, (Oxford University Press, Oxford, 2004),
15. J. H. Nuckolls, Lawrence Livermore National Laboratory, Livermore, CA, Report UCRL-ID-131075 (1988), E. B. Goldman, J. A. Delettrez, and E. I. Thorsos, *Nucl. Fusion* **19**, 555 (1979).
16. J. Nuckolls, J. Emmett, and L. Wood, *Phys. Today* **26**, 46 (1973).
17. C. Stoeckl, R. Boni, F. Ehrne, C. J. Forrest, V. Yu. Glebov, J. Katz, D. J. Lonobile, J. Magoon, S. P. Regan, M. J. Shoup III *et al.*, *Rev. Sci. Instrum.* **87**, 053501 (2016).
18. R. Lauck, M. Brandis, B. Bromberger, V. Dangendorf, M. B. Goldberg, I. Mor, K. Tittelmeier, and D. Vartsky, *IEEE Trans. Nucl. Sci.* **56**, 989 (2009).
19. O. Landoas, V. Yu. Glebov, B. Rossé, M. Briat, L. Disdier, T. C. Sangster, T. Duffy, J. G. Marmouget, C. Varignon, X. Ledoux *et al.*, *Rev. Sci. Instrum.* **82**, 073501 (2011).
20. C. J. Forrest, J. P. Knauer, W. U. Schroeder, V. Yu. Glebov, P. B. Radha, S. P. Regan, T. C. Sangster, M. Sickles, C. Stoeckl, and J. Szczepanski, *Nucl. Instrum. Methods Phys. Res. A* **888**, 169 (2018).
21. X-5 Monte Carlo Team, Los Alamos National Laboratory, Los Alamos, NM, Report LA-UR-03-1987 (2008).

22. P. Doleschall, Phys. Rev. C **69**, 054001 (2004).
23. I. Šlaus, Y. Akaishi, and H. Tanaka, Phys. Rev. Lett. **48**, 993 (1982).
24. S. Oryu, in *Few Body Systems and Nuclear Forces I*, edited by H. Zingl, M. Haftel, and H. Zankel, Lecture Notes in Physics, volume 82 (Springer-Verlag, Berlin, 1978).
25. J. M. Lambert, P. A. Treado, R. G. Allas, L. A. Beach, R. O. Bondelid, and E. M. Diener, Phys. Rev. C **13**, 43 (1976).
26. A. Fujiwara, G. Kamimoto, and A. Tsukamoto, Icarus **31**, 277 (1977).
27. F. Deak, A. Kiss, and J. Kecskemeti, J. Phys. G: Nucl. Phys. **11**, 317 (1985).

Figures

FIG. 1. Diagram of the neutron time-of-flight (nTOF) diagnostic and the location of the OMEGA target chamber. The reaction vessel is positioned 9 cm from the target chamber center using special brackets to minimize neutron scattering from within the target chamber. The detector is shielded from scattered background neutrons with the utilization of a mid-beam collimator (constructed from high-density polyethylene) and the 1-m-thick concrete floor. Neutrons are recorded in current mode using a time-of-flight spectrometer with a large dynamic range, located on the line-of-sight axis downstream of the reaction vessel. PMT: photomultiplier tube.

FIG. 2. Experimental setup with a high-yield neutron source incident on a nuclear reaction vessel positioned 9 cm from target chamber center. The vessel contains non-deuterated or a corresponding deuterated target compounds. Because of the geometry of the reaction volume with respect to the diagnostic instrument, this measurement will cover an emission angle of the breakup neutrons from the reaction vessel in the range $0^\circ \leq \theta \leq 7.4^\circ$, $0^\circ \leq \varphi \leq 2\pi$.

FIG. 3. A comparison of the measured time-of-flight signals clearly indicates the increase in the spectra (1 to 10 MeV) from the breakup of deuterons in the reaction vessel. The excited states of carbon (4.44, 7.65, 9.64 MeV) and oxygen (6.1, 7.0 MeV) are also evident in the spectra.

FIG. 4. Simulations show that a correction is required to infer a cross section only from 14-MeV neutrons. The y axis is the cross section from the neutrons at less than 14 MeV divided by neutrons at 14 MeV. Multiple scattering effects of the neutrons generated in the breakup reaction were modeled using the neutron transport code MCNP simulating details of the experimental setup. This correction uses the cross section in MCNP, which has been shown to be different from the measured cross section.

FIG. 5. Double-differential cross section ($d^2\sigma/d\Omega dE$) for neutron-induced deuteron breakup at 14 MeV using two different reaction vessels with deuterated water (a), deuterated benzene (b), and the averaged values from the separate measurements (c) for a near-zero forward angle. The solid circles are the data reported in this paper, the squares are the data of Brullmann *et al.* [9], and the diamonds are the neutron-induced breakup data of Kecskemti *et al.*, respectively [10]. The solid lines represent Faddeev-type calculation of the neutron-induced deuteron breakup using the realistic CD Bonn + Δ + U1 model, averaged over forward neutron emission angles at $\langle d^2\sigma/dE_n d\Omega_n \rangle_{0^\circ < \theta < 7.4^\circ}$.

TABLE

Table I: Measured and calculated double-differential cross section for the neutron-induced breakup of n - ^2H as a function of E_{lab} from 14-MeV incident neutrons. The theoretical results were obtained solving rigorous 3N Faddeev equations with the realistic CD Bonn + Δ + U1 interaction model.

Energy (MeV)	Measured (D_2O) (mb/sr MeV)	Error (mb/sr MeV)	Measured (C_6D_6) (mb/sr MeV)	Error (mb/sr MeV)	Theory (mb/sr MeV)
0.70	–	–	2.69	6.67	2.43
1.22	1.42	1.98	3.43	3.00	2.46
1.74	4.85	1.50	1.44	1.73	3.00
3.26	5.80	1.88	5.24	0.88	6.15
3.77	9.26	1.80	6.27	1.94	7.80
4.27	11.93	2.00	9.73	1.76	9.84
4.78	14.21	1.91	13.24	1.73	12.13
5.28	14.39	1.86	15.46	1.93	13.99
5.78	12.99	1.78	15.12	1.56	14.07
6.29	13.14	1.97	13.48	1.82	12.63
6.79	11.02	1.47	12.52	1.48	10.86
7.30	10.58	1.30	10.41	1.72	9.38
7.80	10.22	1.08	8.28	1.42	8.21
8.30	8.65	1.15	8.34	1.13	7.30
8.81	7.59	2.67	7.40	1.56	6.58
9.31	8.16	1.02	4.74	6.01	5.95
9.81	6.80	3.43	5.74	1.74	5.40
10.32	4.60	0.86	5.76	3.66	4.96

